Computer-Simulation Study of the Orthorhombic−Hexagonal Phase Change in Lanthanide Manganates ($LnMnO_3$)

Scott M. Woodley,*,† Peter D. Battle,‡ Julian D. Gale,§ and C. Richard A. Catlow†

Davy-Faraday Research Laboratory, The Royal Institution of Great Britain, 21 Albemarle Street, London W1S 4BS, U.K., Inorganic Chemistry Laboratory, University of Oxford, South Parks Road, Oxford OX1 3QR, U.K., and Department of Chemistry, Imperial College of Science, Technology and Medicine, South Kensington SW7 2AY, U.K.

Received September 30, 2002. Revised Manuscript Received January 20, 2003

Static lattice simulation techniques are applied to modeling the structures of the lanthanide manganates ($LnMnO_3$). New interatomic potentials are developed based on the Born model of the ionic solid supplemented by the angular overlap model to describe the nonspherical components of the $Mn^{3+}-O^{2-}$ interactions. The new model correctly predicts the greater stability of hexagonal compared with orthorhombic structures for the system containing the smaller lanthanide ions. A detailed comparison of the simulated structures with experiment is presented.

Introduction

One of the major challenges to theoretical solid-state science is the prediction of the relative stability of different polymorphs. In the present paper we explore the intriguing case of the lanthanide manganates where the structure changes from an orthorhombic perovskite based structure (for the larger lanthanide cations) to a hexagonal structure (for the smaller lanthanide cations); the structures are shown in Figure 1. The aim of the paper is to show that with careful optimization of the potential parameters based on a new type of model, it is possible to describe accurately the changes in structure that occur across the series of compounds.

Background

There have been many successes over the last thirty years in the modeling of oxides using simple interatomic potentials based on the ionic model, particularly when ion polarizability is accounted for via the shell model.[1−6] Such calculations have typically used potentials comprising a Buckingham term to describe the short-range interaction between two ions and a Coulomb term for the long-range interaction. Although potential parameters may be derived theoretically, particularly from fitting to ab initio energy surfaces, most have been obtained by empirical fitting to experimental data including structure and physical properties. However, the Coulomb and Buckingham potentials are purely radial, and consequently can only accurately model structures that contain spherical ions, imposing a significant limitation on the applicability of these methods to transition metal oxides. Even inclusion of the shell model is only capable of representing ions as a dipole, while many transition metal ions possess quadrupolar contributions. The emergence of high-temperature superconductivity and colossal magnetoresistance as major research fields has served to emphasize this limitation because in both cases the compounds in question contain nonspherical, Jahn−Teller active cations, Cu^{2+} and Mn^{3+}, respectively. We have addressed this issue by developing a force field based on the angular overlap model (AOM) which can be used to model nonspherical ions. We have successfully applied this approach to the orthorhombic perovskite $LaMnO_3$,[7] which can be considered as the first member of a series of lanthanide manganese oxides $LnMnO_3$. However a structural change occurs as the radius of the trivalent lanthanide cation decreases, with a hexagonal, nonperovskite phase containing five coordinate Mn^{3+} being formed in high-temperature syntheses for lanthanide cations smaller than Dy^{3+};[8−11]

* To whom correspondence should be addressed via e-mail: smw@ri.ac.uk.
† The Royal Institution of Great Britain.
‡ University of Oxford.
§ Imperial College of Science, Technology and Medicine.

(1) Bell, R. G.; Jackson, R. A.; Catlow, C. R. A. *J. Chem. Soc., Chem. Commun.* **1990**, 782.
(2) Couves, J. W.; Jones, R. H.; Parker, S. C.; Tschaufeser, P.; Catlow, C. R. A. *J. Phys. Condens. Matter* **1993**, *5*, 27, L329.
(3) Catlow, C. R. A.; Bell, R. G.; Gale, J. D. *J. Mater. Chem.* **1994**, *4*, 6, 781.
(4) Bush, T. S.; Gale, J. D.; Catlow, C. R. A.; Battle, P. D. *J. Mater. Chem.* **1994**, *4*, 831.
(5) Taylor, M. B.; Barrera, G. D.; Allan, N. L.; Barron, T. H. K.; Mackrodt, W. C. *Comput. Phys. Commun.* **1998**, *109*, 135.
(6) Davies, R. A.; Islam, M. S.; Chadwick, A. V.; Rush, G. E. *Solid State Ionics* **2000**, *130*, 115.
(7) Woodley, S. M.; Catlow, C. R. A.; Gale, J. D.; Battle, P. D. *J. Chem. Soc., Chem. Commun.* **2000**, *19*, 1879.
(8) van Aken, B. B.; Meetsma, A.; Palstra T. T. M. *Acta Crystallogr. C* **2001**, *57*, 230.
(9) Bertaut, E. F.; Mercier, M. *Phys. Lett.* **1963**, *5*, 27.
(10) Isobe, M.; Kimizuka, N.; Nakamura, M.; Mohri, T. *Acta Crystallogr. C* **1991**, *47*, 423.
(11) Yakel, H. L.; Koehler, W. C.; Bertaut, E. F.; Forrat, E. F. *Acta Crystallogr.* **1963**, *16*, 957.

10.1021/cm021324k CCC: $25.00
Published on Web 03/29/2003

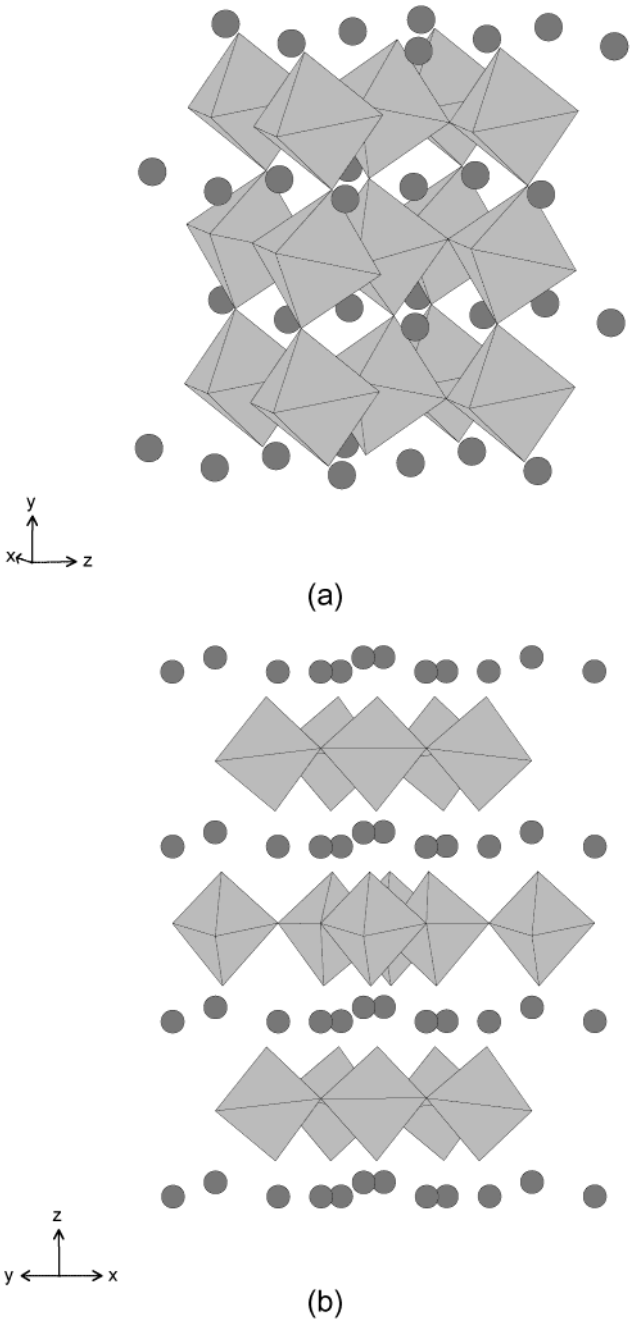

Figure 1. Crystal structure of $LnMnO_3$: (a) Ln = La, (b) Ln = Y. Shaded polyhedra represent (a) MnO_6, (b) MnO_5 groups; filled circles represent Ln.

low-temperature syntheses have allowed the preparation of metastable perovskite phases for Ln = Y, Ho, Er.[12,13] These experimental observations provide data against which we can determine the degree of transferability inherent in our AOM model. The calculations described below show that our model does indeed predict the instability of the perovskite structure for small Ln^{3+} and that, with further scaling, it can give an accurate account of the orthorhombic to hexagonal crossover.

Model

We applied standard lattice-energy minimization techniques to model the $LnMnO_3$ series of compounds. All our results were obtained using the General Utility Lattice Program (GULP).[14,15] The contribution from "spherical" forces between ions to the lattice energy was described by the standard expression

$$E_{\text{spherical}} = \sum_{i,j} \frac{q_i q_j}{4\pi\epsilon_0 r_{ij}} + A_{ij}\, e^{-r_{ij}/\rho_{ij}} - \frac{C_{ij}}{r_{ij}^{\,6}} \qquad (1)$$

where the summation over *i* and *j* includes unique pairs of atoms and their translational images, so as to avoid double counting, within the specified radial cutoff. Three-dimensional periodic boundary conditions were applied to the unit cell. The Ewald summation[16,17] was employed to compute the Coulomb term, using formal charges, *q*, on the ions. The remaining terms constitute the short-range Buckingham potential representing the cation−anion and anion−anion short-range interactions; cutoffs of 12 Å and 10 Å, respectively, were applied. To generate polarization of the oxide ions we used the shell model[18,19] wherein a free ion is described as a point charge coupled by a force constant *k* to a massless shell with charge *Y*. The lattice energy was minimized by relaxing the unit cell dimensions and atomic coordinates at constant pressure using a Newton−Raphson procedure together with the BFGS method[20] of updating the Hessian. In the cases where this procedure found an unstable stationary point, we relaxed the imposed symmetry and applied the rational function optimization[21] method of minimization, which validates that the Hessian is positive definite.

In our calculations, *k*, *Y*, *A*, *ρ*, and *C* for selected interactions were fitted empirically[14] so that the structural parameters of the appropriate phase for one selected member of the $LnMnO_3$ series were reproduced. Assuming the short-range repulsion between the other members of the Ln series and the oxide ions depends only on the differences in the ionic radii of the lanthanide ions, we can calculate the appropriate value of the cation-dependent parameter *A* using the relationship[22]

$$A_1 = A_2 \exp\{(R_1 - R_2)/\rho\} \qquad (2)$$

where R_i are the ionic radii of the Ln^{3+} cations in 8 coordination,[23] as listed in Table 1. Note that the same value of *ρ* is used throughout the series.

The driving force for the distortions of the coordination sphere of Mn^{3+} is associated with the Jahn−Teller effect, which removes a degeneracy in the electronic

(12) Alonso, J. A.; Martínez-Lope, M. J.; Casais, M. T.; Fernández-Díaz, M. T. *Inorg. Chem.* **2000**, *39*, 917.
(13) Brinks, H. W.; Fjellvåg, H.; Kjekshus, A. *J. Solid State Chem.* **1997**, *129*, 334.
(14) Gale, J. D. *Philos. Mag. B* **1996**, *73*, 3.
(15) Gale, J. D. *J. Chem. Soc. Faraday Trans.* **1997**, *93*, 629.
(16) Tosi, M. P. *Solid State Phys.* **1964**, *16*, 1.
(17) Jackson, R. A.; Catlow, C. R. A. *Mol. Simul.* **1988**, *1*, 207.
(18) Dick, B. G.; Overhauser, A. W. *Phys. Rev.* **1958**, *112*, 90.
(19) Dove, M. T. *Introduction to Lattice Dynamics*; Cambridge Press: Cambridge, U.K., 1993.
(20) Press, W. H.; Teukolsky, S. A.; Vetterling, W. T.; Flannery, B. P. *Numerical Recipes*, 2nd ed.; Cambridge University Press: Cambridge, U.K., 1992.
(21) Cormack, A. N.; Lewis, G. V.; Parker, S. C.; Catlow, C. R. A. *J. Phys. Chem. Solids* **1988**, *49*, 1, 53.
(22) Banerjee, A.; Adams, N.; Simons, J.; Shepard, R. *J. Phys. Chem.* **1985**, *89*, 52.

Table 1. Ionic Radii of Ln^{3+} in 8 Coordination and Two Sets of Scaled Potential Parameters (A_{ij}) for the Born−Mayer Interaction $Ln^{3+}-O^{2-}$ Generated from Equation 2[a]

rare earth Ln	ionic radius[23] (pm)	Set A *A* (eV)	Set B *A* (eV)
La	130.0	4317.17	18334.64
Ce	128.3	4078.30	17166.92
Pr	126.6	3852.65	16073.57
Nd	124.9	3639.48	15049.86
Pm	123.3	3449.63	14146.00
Sm	121.9	3291.66	13399.77
Eu	120.6	3151.45	12742.13
Gd	119.3	3017.22	12116.76
Tb	118.0	2888.71	11522.09
Dy	116.7	2765.67	10956.61
Y	115.9	2692.57	10622.50
Ho	115.5	2656.75	10459.29
Er	114.4	2560.68	10023.26
Tm	113.4	2476.36	9642.67
Yb	112.5	2402.85	9312.51
Lu	111.7	2339.34	9028.54

[a] Set A is scaled ($\rho = 0.298662$ Å) from $A_{ij}(La^{3+}-O^{2-})$ as fitted to orthorhombic $LaMnO_3$, and set B is scaled ($\rho = 0.258328$ Å) from $A_{ij}(Y^{3+}-O^{2-})$ as deduced from simultaneous fitting of orthorhombic and hexagonal $YMnO_3$.

energies. To model the irregular coordination geometry associated with these "non-spherical" ions, we chose to add a contribution to the lattice energy that corresponds to this energy-level splitting:[24]

$$E_{JT} = \sum_{tsd} \epsilon_d^t (O_d^{ts} - 1) \tag{3}$$

Here, ϵ_d^t and O_d^{ts} are the energy changes and occupations of the *d*-orbitals for each transition metal *t*, respectively,[24] and *s* is the spin of an electron. An adaptation of the angular overlap model (AOM) is used to obtain ϵ_d^t. Basically, we compute the eigenvalues, ϵ_d^t, of a 5×5 overlap matrix, $H_{dd'}$, for each transition metal ion. $H_{dd'}$ is formed by taking the products of the angular contributions to the overlap integrals, Γ_d,[25] between the transition metal ion *d*-orbital and the orbitals of any surrounding ligand

$$H_{dd'} = \sum_l R\Gamma_d\Gamma_{d'} \tag{4}$$

where the Born−Mayer interaction is used to model the radial dependence of the interaction between the transition metal and its ligand

$$R = B \exp(-r/p) \tag{5}$$

The two new parameters, *B* and *p*, depend on ligand type and can be empirically fitted. Upon optimization of the lattice energy with respect to the cell parameters and ionic coordinates, the energy levels may become degenerate and the order of the energy levels may also change. To prevent the energy landscape becoming discontinuous, we allow partial occupancies (or a nonzero probability that an electron can populate a higher energy state) via the implementation of a Fermi function. Further details of the theory of the AOM and its application to manganates are given in ref 24.

(23) Source: WebElements [http://www.webelements.com/].
(24) Woodley, S. M.; Battle, P. D.; Catlow, C. R. A.; Gale, J. D. *J. Phys. Chem. B* **2001**, *105*, 29, 6824.
(25) Bridgeman, A. J.; Gerloch, M. *Prog. Inorg. Chem.* **1997**, *45*, 179.

Table 2. Percentage Differences between Observed[12] and Calculated Lattice Parameters of Orthorhombic $LnMnO_3$ Following Lattice Energy Minimization Using the Potential Parameters Sets P, A, and B

Ln	set	volume	*a*	*b*	*c*
La	P	1.65	0.47	−0.20	1.38
	A	0.26	−0.14	0.03	0.37
	B	−0.94	−0.42	−3.63	3.23
Pr	P	−0.86	0.45	−1.48	0.18
	A	0.37	0.57	−1.18	0.99
	B	0.52	1.31	−2.96	2.25
Nd	P	−0.91	0.77	−1.94	0.28
	A	−0.03	0.52	−2.03	1.51
	B	0.64	1.46	−2.77	2.03
Tb	P	52.34	87.53	−7.86	−11.83
	A	0.32	−1.26	−6.99	9.24
	B	1.15	1.82	−2.38	1.77
Dy	P				
	A	0.27	−1.68	−7.70	10.48
	B	1.04	1.64	−2.63	2.09
Y	P	66.71	10.18	5.80	43.01
	A	7.47	−33.54	3.99	55.49
	B	1.98	2.04	−2.37	2.37
Ho	P				
	A	6.22	−33.85	3.21	55.58
	B	0.61	2.15	−2.79	1.31
Er	P	66.05	12.67	39.02	23.52
	A	6.74	−33.80	3.43	55.88
	B	1.57	2.05	−2.86	2.46

Derivation of Potential Parameters

Three sets of potentials describing the Ln−O interaction were used in modeling the structures of two $LnMnO_3$ phases that are shown in Figure 1. First we used the potential data that are available in the literature;[4,7] these are referred to as set P and they do not cover all the Ln elements. To generate a second set of potential parameters for the $Ln^{3+}-O^{2-}$ interaction we took the parameters previously fitted for orthorhombic $LaMnO_3$,[7] and applied eq 2 in order to allow for the variation of cation radius. Note that the orthorhombic, as opposed to the cubic, perovskite phase has 4 per unit cell rather than 1 corner sharing MnO_6 octahedra that have rotated as shown in Figure 1. The resulting potential parameters are presented in Table 1 as set A. As we will show, this set was not able to predict the orthorhombic phase to be more stable than that of the hexagonal structure for the earlier members of the lanthanide manganate series $LnMnO_3$. We therefore generated a second set (B) of scaled potential parameters by simultaneous fitting to both the orthorhombic and hexagonal phases of $YMnO_3$,[8,12] followed by scaling using eq 2.

Results

Potential Set P. The percentage differences in the lattice parameters, shown in Table 2, quite clearly show that for the larger Ln elements potential set P produces a reasonable agreement with the experimental data. However, for the lanthanides with smaller radii (Ln = Y, Er) the observed orthorhombic phase is calculated to be unstable. The $Ln^{3+}-O^{2-}$ interactions in set P were originally fitted[4] to reproduce the respective binary oxide structures, and for the larger Ln, where the orthorhombic phase was found to be stable, the coordi-

Table 3. Mn−O Bond Lengths in $LnMnO_3$ Calculated Using Potential Set A

R	Mn−O1 (Å)			Mn−O2 (Å)			*d* (Å)[a]	space group[b]
La	1.97	1.97	1.90	1.90	2.18	2.19	0.28	*Pbnm*
Ce	1.97	1.97	1.90	1.90	2.19	2.19	0.29	*Pbnm*
Pr	1.97	1.97	1.90	1.90	2.19	2.19	0.29	*Pbnm*
Nd	1.99	1.99	1.89	1.89	2.17	2.17	0.28	*Pbnm*
Pm	2.02	2.02	1.88	1.88	2.14	2.15	0.27	*Pbnm*
Sm	2.06	2.06	1.88	1.88	2.11	2.11	0.24	*Pbnm*
Eu	2.09	2.09	1.88	1.88	2.09	2.09	0.21	*Pbnm*
Gd	2.11	2.11	1.88	1.88	2.06	2.06	0.23	*Pbnm*
Tb	2.13	2.13	1.89	1.89	2.04	2.04	0.24	*Pbnm*
Dy	1.79		1.79	2.02	2.02	2.02		$P6_3/mmc$
Y	1.79		1.79	2.01	2.01	2.01		$P6_3/mmc$
Ho	1.79		1.79	2.01	2.01	2.01		$P6_3/mmc$
Er	1.83		1.76	1.78	1.92			$P2_12_12_1$
Tm	1.84		1.76	1.78	1.92			$P2_12_12_1$
Yb	1.84		1.76	1.78	1.92			$P2_12_12_1$
Lu	1.84		1.76	1.78	1.92			$P2_12_12_1$

[a] *d* is the maximum bond difference within the MnO_6 octahedra and thus an indication of the distortion. [b] The space group after unconstrained optimization was obtained using CERIUS[2] with the tolerance set to 0.1 Å.

nation number of Ln in both the binary oxide and orthorhombic $LnMnO_3$ is 8. However, for the smaller lanthanides the coordination number in the binary oxide is 6. Thus the $Ln^{3+}-O^{2-}$ interaction potential can only be considered to be transferable when the Ln coordination number is constant.

Potential Set A. Potential set A was initially used to model only the orthorhombic $LnMnO_3$ (Ln = La, Pr, Nd, Tb, Dy, Y, Ho, Er) phases reported by Alonso et al.[12] As in the case of potential set P, when $LnMnO_3$ was modeled with potential set A one of two forms of behavior was found depending on the radius of Ln: the lanthanides with the larger radii remained in the orthorhombic phase upon relaxation, while those with the smaller radii did not. However, there was one important difference in the results produced by the two sets of potentials. In the case of set A, the local energy minimum found for the lanthanides with the smaller radii corresponded to the hexagonal phase (i.e., the phase that is observed to be more stable for these smaller cations) whereas set P produced a nonphysical structure.

The calculations described above were performed in the conventional manner; i.e., the calculated structure of $LnMnO_3$ was generated using the observed structure of orthorhombic $LnMnO_3$ as a starting point for the energy minimization. To be able to consider compounds formed by all the lanthanide elements, rather than just the subset used by Alonso et al (i.e., including Ce, Pm, Sm, Eu, Gd, Tm, Yb, Lu), we calculated the structure of each $LnMnO_3$ phase using the $LaMnO_3$ structure as the starting point for each optimization. The results of the simulation of $LnMnO_3$ from orthorhombic $LaMnO_3$ are shown in Table 3 and Figure 2. Initially, as the Ln ionic radius decreases, we found that the distortion of the MnO_6 octahedra grew as the lattice parameters decreased. The decrease in the distortion of the MnO_6 groups as the internal or chemical pressure is reduced matched that observed by Alonso et al.[12] We note that when external pressure is applied then the distortion of the MnO_6 groups decreases. As the ionic radius of Ln decreases beyond that of Nd, our calculations predicted a gradual change in the principal axis of the

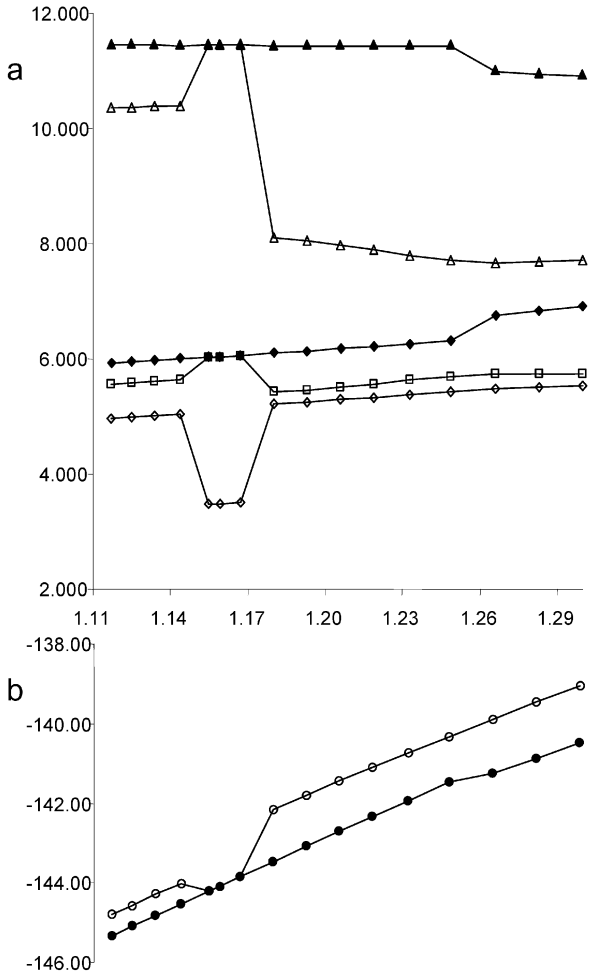

Figure 2. (a) Lattice parameters (Å) and (b) lattice energies (eV/mol. $LnMnO_3$) of $LnMnO_3$ as a function of ionic radius (Å) for Ln^{3+} calculated using potential set A. Open and filled diamonds, squares, triangles, and circles show the values of *a*, *b*, *c*, and *E* obtained by relaxing the orthorhombic $LaMnO_3$ structure and the hexagonal $YbMnO_3$ structure, respectively.

distortion (Table 3) that is not observed by Alonso et al. The orthorhombic phase of $LaMnO_3$ minimized to give the hexagonal phase for $DyMnO_3$, $YMnO_3$ and $HoMnO_3$, as had simulations that used orthorhombic $LnMnO_3$ as a starting point (N. B. The changes in unit cell parameter seen in Figure 2 are as follows: $\sqrt{3}\, a_{orth} \leftrightarrow a_{hex}$, $b_{orth} \leftrightarrow b_{hex}$, $c_{orth} \leftrightarrow c_{hex}$, $4\gamma_{orth} \leftrightarrow 3\gamma_{hex}$). Once again the simulations predicted the phase transition at approximately the correct point in the lanthanide series. However, for the smallest cations, the direct minimization of the lattice energy became trapped in a local minimum and the hexagonal phase was not reached. The local minimum was centered on a hitherto unobserved orthorhombic structure containing 4-coordinate Mn. We give the structural data for the smallest cation in Table 4. As we had initialized each optimization with the observed structural parameters of $LaMnO_3$, we expect a greater decrease from the initial unit cell volume for each successive member of the $LnMnO_3$ series from Ln = La to Lu. More specifically for Ln = Ce to Lu, we have relaxed a set of expanded structures, that is, we have crudely simulated the effect of heating, most significantly for the orthorhombic compounds containing the smaller lanthanides, a point to which we will return below. We also calculated the structure of

Table 4. Relaxed Structural Parameters for $LuMnO_3$ (space group $P2_12_12_1$)[a] Following Lattice Energy Minimization Using the Potential Parameters Set A and the Initial Starting Structural Parameters for Orthorhombic $LaMnO_3$

	x	*y*	*z*
Lu	0.2897	0.0779	0.7771
Mn	0.7849	0.1155	0.5657
O1	0.0337	0.7688	0.8034
O2	0.5676	0.9073	0.3558
O2	0.0336	0.1220	0.4455

[a] $a = 4.974$ Å, $b = 5.553$ Å, $c = 10.352$ Å.

each $LnMnO_3$ phase using the hexagonal $YbMnO_3$ structure as a starting point for all $LnMnO_3$ compositions. In this case, no phase transition to a perovskite structure was found for any $LnMnO_3$ composition (Figure 2), the lattice energy of the hexagonal phase always being lower. The hexagonal phase has ionic layers where the manganese ions are 3 coordinated with the oxide ions, forming a hexagonal lattice in the *ab*-plane. For Ln = La, Cr, Pr our calculated structures predict a distortion of these layers; the oxide ions move within each layer such that smaller discrete Mn_3O_3 rings are formed. It is thus clear that the apparent degree of success of set A is dependent on the starting point chosen, and that these simulations do not give a reliable description of the energetics.

Potential Set B. The lattice parameters calculated for $YMnO_3$ in the derivation of parameter set B were within 2.4% of the observed values for both the orthorhombic and hexagonal phases. This level of agreement was achieved by using the potential parameters of Catlow et al.[26] for the interaction between oxygen shells, but with a slightly higher spring constant of $k = 91.0$ eV Å^{-2}. The parameters for the interactions between the manganese and oxide ions were also refined to values of A = 1700.0 eV, $\rho = 0.325419$ Å, B = 30.66 eV, and $p = 0.322555$ Å. Having modified the Ln−O interaction by scaling (eq 2), these parameters were then tested by performing an optimization of the orthorhombic $LnMnO_3$ structures reported by Alonso et al. In contrast to the results of the corresponding calculations using parameter set A, all the structures were found to be energetically stable (Table 2) without significant distortion of the local minimum, and the maximum change in any lattice parameter was −3.6% for $LaMnO_3$; no other change was greater than 3%. Parameter set B was then used to investigate the full range of $LnMnO_3$ compositions for both orthorhombic and hexagonal symmetry (Figure 3). The appropriate experimentally determined structural parameters for $YMnO_3$ were used as a starting point for each calculation. The calculations showed, in this case, that the orthorhombic phase became more stable at a cation radius close to that of Nd^{3+}, as shown in Figure 3(b). This is a great improvement compared to the results generated using parameter set A where the hexagonal phase was always found to be the more stable. However, in contrast to the results obtained with parameter set A, two distinct sets of unit cell parameters exist on both sides of the energy crossover. This shows that an energy barrier exists between the two phases in the case of set B, whereas

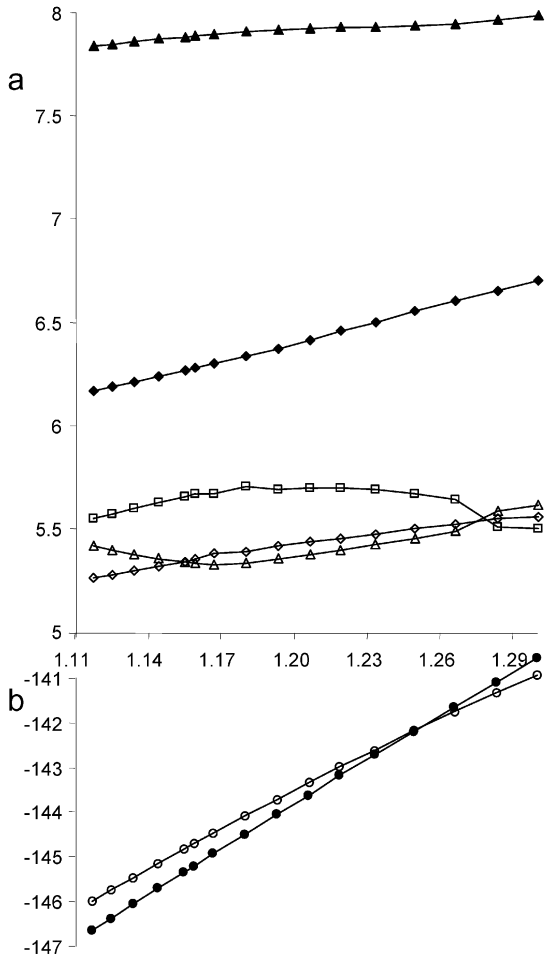

Figure 3. (a) Lattice parameters (Å) and (b) lattice energies (eV/mol. $LnMnO_3$) of $LnMnO_3$, as a function of ionic radius (Å) for Ln^{3+}, calculated using potential set B. Open diamonds, squares, and triangles represent the *a*, *b*, $c/\sqrt{2}$ lattice parameters of the orthorhombic phase, and filled diamonds and triangles represent the *a* and $c/\sqrt{2}$ lattice parameters for the hexagonal phase. Open and filled circles represent the lattice energy of orthorhombic and hexagonal phases, respectively.

the equivalence of the unit cell parameters and lattice energy in the case of set A for Ln = Dy, Y, Ho shows that only a single energy minimum exists.

Discussion

Insight into the problems of generating distinct local energy minima corresponding to the orthorhombic and hexagonal phases for set A, Ln = Dy, Y, Ho, is gained by modeling the Ln pyrochlores, $Ln_2Mn_2O_7$ which contain no nonspherical Mn^{3+} ions. The pyrochlore structure is more stable than that of the orthorhombic perovskite structure; the end member $Lu_2Mn_2O_7$ is reported to be stable up to 800 °C (after which it loses oxygen to form hexagonal $LuMnO_3$).[27] We can therefore assume that the local energy minimum is contained within a deeper well. The Buckingham parameters for Mn^{4+}−O^{2-} and Tl^{3+}−O^2 were previously refined to reproduce the structures of their respective binary oxides and were then used to model successfully Tl_2-

(26) Catlow, C. R. A. *Proc. Royal Soc. London A* **1977**, *353*, 533.

(27) Subramanian, M. A.; Torardi, C. C.; Johnson, D. C.; Pannetier, J.; Sleight, A. W. *J. Solid State Chem.* **1988**, *72*, 24.

Mn_2O_7.[28] The differences ($a_{calc} - a_{obs}$) between our calculated lattice parameters for the pyrochlores and those observed[27] are between −1.4 and −1.5% for Ln = Y, Dy−Lu. The fact that the difference is always negative, whereas for $Tl_2Mn_2O_7$ the difference was +0.25%, suggests that we underestimated the radius of the Ln cation for these ions. As described above, decreasing the cation size simulates the effect of starting the energy calculation at a relatively high temperature. Underestimating the radius of Ln thus places us in a regime where the energy barrier between phases may be overcome.

Because parameter set B (but neither set P nor set A) reproduces the change in relative stability of the orthorhombic and hexagonal phases, the remainder of our discussion will focus on set B. In the following analysis of the structural properties of the orthorhombic phase of $LnMnO_3$ we mirror the approach developed by Alonso et al.[12] in comparing the results of our simulations with experiment.

(i) Lattice Parameters. We found the lattice parameters for the hexagonal phase generally scaled linearly with the Ln ionic radii. Over the range of lanthanide radii where comparison is possible, our simulated orthorhombic lattice parameters displayed the same qualitative trend as those observed by Alonso et al: that is, *a* and *c* increased with increasing ionic radius, whereas *b* reached a maximum and then decreased. They reported that as the lanthanide ionic radii changed, the MnO_6 octahedra rotated and distorted in order to keep the *b* parameter roughly constant. The Mn−O−Mn bond angles give a measure of how far the MnO_6 octahedra have rotated. If all the MnO_6 octahedra are perfectly aligned parallel to each other then a bond angle of 180° would result. The upper part of Figure 4 shows our simulated bond angles as a function of the lanthanide ionic radii. Clearly, the degree of rotation of the MnO_6 octahedra increased from $LaMnO_3$ to $LuMnO_3$. Note that there are two curves as there are two unique oxygen sites.

(ii) Octahedral Distortion. It has been proposed[12] that if the distortion within the perovskite is driven by steric effects then $a < c/\sqrt{2} < b$, and when the distortion is driven by Jahn−Teller (JT) effects then $c/\sqrt{2} < a < b$. If we follow this scheme, then our calculations suggest that for Ln = Y−Pr the distortions are driven by JT effects, whereas for Ln = Lu−Ho steric effects begin to dominate. For Ln = Y, there was a small difference between $c/\sqrt{2}$ and *a*, which was probably directly related to the fact that the simulated distortion within the MnO_6 octahedra was smaller than that observed. We note that when fitting the parameters, increasing the JT term (see eq 5) did increase this distortion, but at a cost of increasing the errors in the lattice parameters of the hexagonal phase. For Ln = Ce and La, the *b* parameter was less than both *a* and $c/\sqrt{2}$, an indication perhaps that these end members have remained in a higher energy state. However, if the observed structural parameters for $LaMnO_3$ are used as a starting point, rather than those for $YMnO_3$, then after relaxation a larger value of *b* is obtained. Moreover, comparing the tilt of the MnO_6 octahedra in both relaxed structures we found a difference of ∼1°. This final difference is much smaller than the initial difference in the two starting structures (11°) but nevertheless suggested that as the structural parameters of $YMnO_3$ were relaxed, the rotation of the octahedra became trapped in a higher local energy minimum.

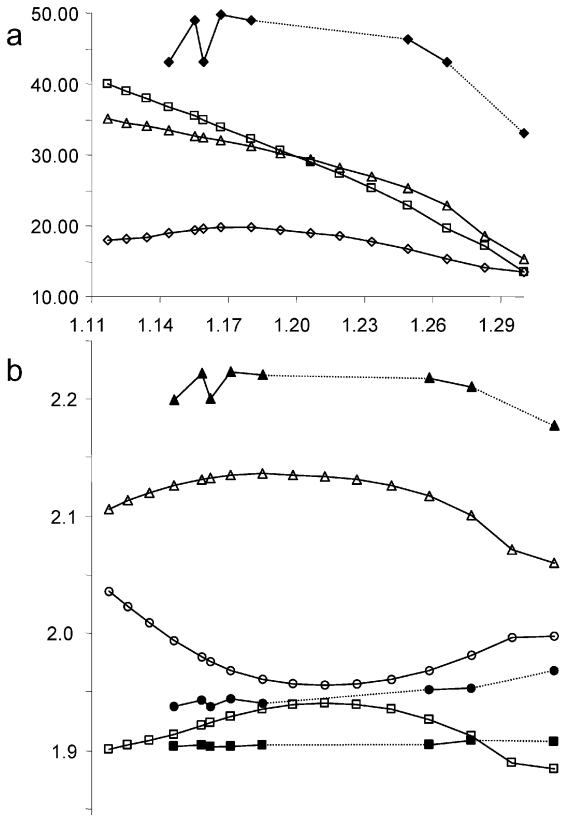

Figure 4. Structural parameters of orthorhombic $LnMnO_3$ as a function of ionic radius (Å) for Ln^{3+}. The triangles and squares in (a) are the complement of the bond angle Mn−O−Mn, and the open and filled diamonds represent the simulated and observed distortion parameter Δ_d (defined in eq 7). The circles, triangles, and squares in (b) represent the simulated (open symbols) and observed[12] (filled symbols) Mn−O bond values within the MnO_6 octahedra.

(iii) Orthorhombic Strain. The orthorhombic strain, due to both the steric and JT effects, is defined as

$$s = 2(b - a)/(a + b) \qquad (6)$$

Furthermore, it is straightforward to calculate the lattice parameters as if the MnO_6 were just rotated and not distorted in any way (so removing any JT effect) and thus compute the orthorhombic strain, *s′*, due to just steric effects (see Alonso et al). In Figure 5(a) we plot *s*, *s′* and $s - s'$ (representing the JT effect) as a function of Ln^{3+} ionic radii for our simulated model of orthorhombic $LnMnO_3$. This graph shows that when the ionic radius for Ln^{3+} is larger than that for Y^{3+} the strain on the perovskites is influenced by the JT effect ($s - s' > s'$), whereas for Ln^{3+} it is smaller than for Y^{3+}, and so steric effects dominate ($s' > s - s'$). We should note also the continuous decrease in the orthorhombic strain due to steric effects as the lanthanide ionic radius decreases. Again, the sudden drop in the JT effect for Ln = Ce and Ln = La is a consequence of modeling their

(28) Woodley, S. M.; Battle, P. D.; Gale, J. D.; Catlow, C. R. A. *Phys. Chem. Chem. Phys.* **1999**, *1*, 2535.

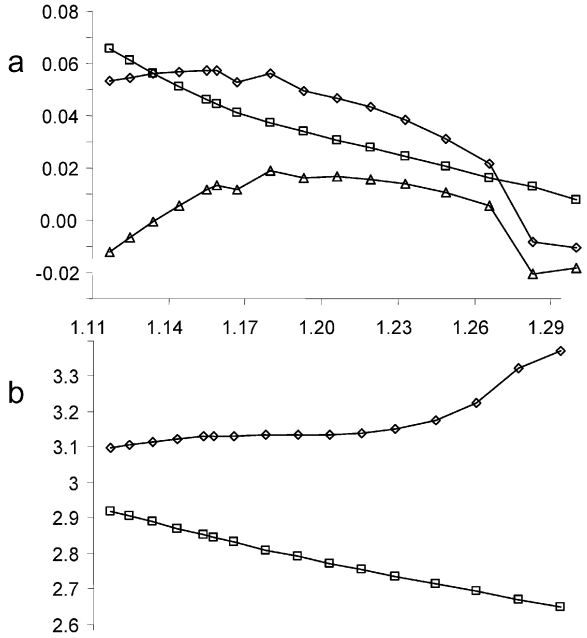

Figure 5. (a) Spontaneous orthorhombic strain (diamonds, *s*) in $LnMnO_3$ due to steric effects (squares, *s′*) and JT effects (triangles, *s*-*s′*) as a function of ionic radius (Å) for Ln^{3+}. (b) Bond valence for Mn in simulated orthorhombic (diamonds) and hexagonal (squares) $LnMnO_3$ as a function of ionic radius for Ln^{3+}.

respective orthorhombic structures with values of *b* smaller than *a* and *c* (as discussed above).

(iv) Mn−O Bond Distances. The Mn−O bond distances, d_n, in the MnO_6 octahedra are shown in Figure 4, together with the distortion parameter[12]

$$\Delta_d = \frac{1}{6}\sum_{n=1}^{6}\left(\frac{d_n - \langle d\rangle}{\langle d\rangle}\right)^2 \qquad (7)$$

There is good qualitative agreement between that simulated using the scaled potential parameters (set B) and that observed (with the exception that for the shorter bonds we simulated a greater variation). For example, the longest bond, *l*, increases then levels off as the ionic radius decreases from La to Ho. Our simulations then suggest that *l* decreases for the latter members down to Ln = Lu. Although our values for Δ_d are less than half of those observed (again due to requiring a reasonable fit to both the orthorhombic and hexagonal phases) we do find that Δ_d increases up to and including Ln = Dy. Then, Δ_d gradually decreases from Ln = Dy to Lu. Alonso et al reported that Δ_d was low for Ln = Y and Er (Δ_d = 49.7, 43.1, 48.9, 43.0 for Ln = Dy, Y, Ho, Er, respectively). The calculated variation of Δ_d is consistent with the suggestion that the smaller observed values of Δ_d for Ln = Y and Er are due to the presence of some Mn^{4+} (which was not included in the calculation and for which Δ_d would equal zero). It was suggested by Brinks et al,[13] that some Mn^{4+} content probably helps to stabilize the orthorhombic phase when the distortion of the MnO_6 is largest.

From the Mn−O bond distances within the MnO_6 octahedra, Alonso et al calculated the bond valence[12] for the Mn cation. For the various orthorhombic $LnMnO_3$ structures that they investigated, we calculate the bond valence to be between 3.12 and 3.16, except for the two smallest members (Ln = Y and Er) where it is 3.21 and 3.25, respectively. Alonso et al inferred that the increase in the bond valence indicated that there was a small amount of Mn^{4+} in their samples of $YMnO_3$ and $ErMnO_3$. In modeling the structures for $LnMnO_3$ we did not include any Mn^{4+} content. In the lower part of Figure 5 we plot the bond valences for the manganese ion in our simulated structure. From Ln = La to Lu, we do not find a significant increase in the bond valence for any member, thereby again confirming their observation. In contrast, we calculate that the bond valence for the manganese ion within the hexagonal phase is less than 3 and scales linearly as a function of the lanthanide ionic radius. Moreover, the difference in the calculated Mn bond valence curves for orthorhombic and hexagonal $LnMnO_3$ diverged as the ionic radius for Ln^{3+} increased.

Table 5. Observed and Calculated Lattice Parameters and Mn−O Bond Lengths of Hexagonal $YbMnO_3$ Following Lattice Energy Minimization Using the Potential Parameters Set B

	V (Å^3)	*a* (Å)	*b* (Å)	*c* (Å)
observed[29]	360.974	6.0584	6.0584	11.3561
calculated	367.731	6.185	6.185	11.099
		Mn−O (Å)		
observed[29]	1.867	1.868	2.039	2.034[2]
calculated	1.8399	1.8398	2.0784	2.0675[2]

The Mn−O bond lengths observed[29] and calculated for the MnO_5 pyramid of a representative hexagonal phase, $YbMnO_3$, are listed in Table 5. This member of the family is chosen as an example because it has been the subject of a structure determination by single-crystal X-ray diffraction and the ionic radius of Yb^{3+} is significantly different from that of Y^{3+}, which was used in the optimization of the parameter set. The tabulated data show that the quality of the simulation of the hexagonal structure is at least as good as that of the orthorhombic materials. The maximum percentage difference between the observed and calculated bond lengths is 1.9%.

Conclusion

This study has shown that with Born model interatomic potentials, when modified by inclusion of the angular overlap model to describe Mn^{3+}−O^{2-} interactions, it is possible to reproduce both the gross and the more subtle features of the structural changes which occur across the $LnMnO_3$ series. Such methods require that careful attention is paid when optimizing the Ln^{3+}−O^{2-} parameters and should now be able to probe detailed aspects of the structural chemistry of complex ternary oxides.

Acknowledgment. We thank the EPSRC for funding this project and for the provision of computer resources, and Accelrys Inc. for provision of Cerius[2] software.

CM021324K

(29) van Aken, B. B. Ph.D. Thesis, University of Groningen, The Netherlands, 2001.